Available online at www.sciencedirect.com
SCIENCE DIRECT®
Catalysis Today 105 (2005) 173–179
CATALYSIS TODAY
www.elsevier.com/locate/cattod

The effectiveness factor for zeolite catalysed reactions

R. Baur, R. Krishna *

Van't Hoff Institute for Molecular Sciences, University of Amsterdam, Nieuwe Achtergracht 166, 1018 WV Amsterdam, The Netherlands

Abstract

The Langmuir–Hinshelwood (LH) rate expression is often used to describe the kinetics of heterogeneously catalyzed reactions using zeolites. A factor $\theta_V \equiv [1 - \sum_i \theta_i]$ in the LH expression allows for the reduction of the reaction rate with increased fractional occupancies θ_i of the individual species on the surface. Most commonly in practice the multi-component Langmuir (MCL) approach is used for calculation of the fractional occupancies giving $\theta_V \equiv 1/[1 + \sum_i b_i f_i]$ where the b_i are the Langmuir adsorption constants and f_i are the component fugacities in the gas phase. The LH–MCL approach is however thermodynamically consistent only when the saturation capacities of all the individual species in the mixture are identical to one another, or when the component loadings are small. For mixtures containing molecules with different saturation capacities, the sorption loadings are significantly affected by entropy effects, especially for high loadings within the zeolite catalyst. In the general case, we need to determine the sorption loadings, and occupancies, using the Ideal Adsorbed Solution Theory (IAST). Using the gas phase isomerization of *n*-hexane with MFI zeolite catalyst as an illustration we demonstrate the limitations of the LH–MCL kinetics for calculation of the catalyst effectiveness factor. The differences between the classical LH–MCL and LH–IAST approaches increase at high loadings inside the catalyst pellet. The important consequences for design of fixed bed reactors are also illustrated.

Keywords: Zeolite catalysis; Isomerization; Molecular simulations; Packed bed reactor; Effectiveness factor; Langmuir–Hinshelwood kinetics; Ideal Adsorbed Solution Theory; Entropy effects; MFI zeolite

1. Introduction

Zeolites are widely used in the chemical industries to catalyze a variety of reactions such as cracking, oxidation (hydro)isomerization, alkylation and esterification [1–3]. Consider, for example, the reversible isomerization reaction $A_1 \rightleftarrows A_2$ taking place in a zeolite catalyst. At chemical equilibrium we know from thermodynamic considerations that the Gibbs free energy is minimized. If the forward and backward reactions are both considered to be first order, we obtain at chemical equilibrium in terms of fugacities, f_i, the relation:

$$k_f f_1 - k_b f_2 = 0 \tag{1}$$

where the subscripts 1 and 2 refer to A_1 and A_2. The forward and backward reaction rate constants k_f and k_b have the units $Pa^{-1}\,s^{-1}$. The left hand side of Eq. (1) represents the chemical driving force. The essential idea of the Langmuir–Hinshelwood (LH) reaction rate expression that is commonly used to describe the heterogeneously catalysed kinetics is that the reaction rate is proportional to this chemical driving force and also proportional to the fractional *vacancy*, $\theta_V = (1 - \theta_1 - \theta_2)$ on the catalyst surface [4], i.e.

$$r = (k_f f_1 - k_b f_2)\theta_V = (k_f f_1 - k_b f_2)(1 - \theta_1 - \theta_2) \tag{2}$$

This expression anticipates that the reaction rate decreases when the total occupancy on the catalyst surface increases, i.e. the vacancy θ_V is reduced. It is to be noted that the L–H expression (2) is general and does not refer to any specific way of calculating the component occupancies θ_i on the catalytic surface. In the chemical reaction engineering

* Corresponding author. Tel.: +31 20 5257007; fax: +31 20 5255604.
E-mail address: r.krishna@uva.nl (R. Krishna).

0920-5861/$ – see front matter © 2005 Elsevier B.V. All rights reserved.
doi:10.1016/j.cattod.2005.04.007

Nomenclature

b_i	parameter in the Langmuir adsorption isotherm (Pa^{-1})
c_i	molar concentration of species i (mol m^{-3})
$Đ_i$	Maxwell–Stefan diffusivity of species i in zeolite ($m^2\ s^{-1}$)
$Đ_{ij}$	Maxwell–Stefan diffusivity describing interchange between i and j ($m^2\ s^{-1}$)
DF	Driving force defined in Eq. (13) (dimensionless)
f_i	fugacity of species i (Pa)
k_f	forward reaction rate constant ($Pa^{-1}\ s^{-1}$)
k_b	backward reaction rate constant ($Pa^{-1}\ s^{-1}$)
L	Length of packed bed (m)
N_i	molar flux of species i (mol $m^{-2}\ s^{-1}$)
p_{i0}	partial pressure of species i at reactor inlet (Pa)
$q_{i,sat}$	saturation loading of component i (mol kg^{-1})
r	reaction rate (s^{-1})
u_0	interstitial fluid velocity in packed bed at inlet (m s^{-1})

Greek letters

Θ_i	molecular loading of species i (molecules per unit cell)
$\Theta_{i,sat}$	saturation loading of species i (molecules per unit cell
δ	radius of the spherical catalyst (m)
ε	porosity of packed bed of zeolite catalyst (dimensionless)
ϕ	classical Thiele Modulus defined in Eq. (12) (dimensionless)
μ_i	molar chemical potential (J mol^{-1})
ν_i	stoichiometric coefficient (dimensionless)
θ_i	fractional occupancy of component i (dimensionless)
θ_V	vacancy (dimensionless)
ρ	zeolite density (kg m^{-3})
τ	dimensionless residence time (dimensionless)
ξ	dimensionless diffusion path (dimensionless)

Subscripts

0	referring to inlet of reactor
1	referring to species 1
2	referring to species 2
A	referring to site A
B	referring to site B
i	referring to species i
s	referring to surface of particle
sat	referring to saturation conditions
V	referring to vacant sites in zeolite

literature, e.g. [4], however, a more restrictive form of the L–H formulation is usually presented in which the multi-component Langmuir (MCL) isotherm is used to calculated the component occupancies from information on the bulk fluid phase fugacities f_i:

$$\theta_i \equiv \frac{\Theta_i}{\Theta_{i,\mathrm{sat}}} = \frac{b_i f_i}{1 + b_1 f_1 + b_2 f_2}, \quad i = 1, 2; \qquad \theta_V = 1 - \theta_1 - \theta_2 = \frac{1}{1 + b_1 f_1 + b_2 f_2} \tag{3}$$

where Θ_i are the molar loadings, $\Theta_{i,\mathrm{sat}}$ are the saturation capacities and the b_i are the Langmuir adsorption constants. Combining Eqs. (2) and (3) we obtain the commonly used expression:

$$r = \frac{k_f f_1 - k_b f_2}{1 + b_1 f_1 + b_2 f_2} \tag{4}$$

The expression (4) is often presented with the component partial pressures p_i in place of the fugacities f_i. The expression $1/(1 + b_i f_i + b_2 f_2)$, which equals the fractional vacancy θ_V, is the factor by which the actual reaction rate on the surface is reduced. We shall call Eq. (4) the LH–MCL approach to emphasise clearly that the occupancies are calculated using the specific MCL model.

In practice, there are some important limitations of the MCL approach, Eq. (3), for calculation of the occupancies of the species. Firstly, the adsorption of molecules in many zeolites show inflection behaviour that can only be captured by use of a *multi*-site Langmuir model [5–8]. As illustration let us consider adsorption of hexane isomers, *n*-hexane (*n*C6), 3-methylpentane (3MP) and 2,2-dimethylbutane (22DMB) in MFI zeolite, that consists of a set of straight channels (0.53–0.56 nm wide), intersecting with zig-zag channels (0.51–0.55 nm wide). Configurational-Bias Monte Carlo (CBMC) simulations of the pure component sorption isotherms of hexane isomers [9,10] in MFI at 362 K are shown in Fig. 1a. The accuracy of the CBMC calculation techniques have been verified in several publications [9–12] in which comparisons are made with experimental data. The linear *n*C6 molecule has a chain length that is commensurate with the length of the zig-zag channels and a maximum of eight molecules per unit cell can be accommodated. The configuration of di-branched 22DMB is such that these bulky, yet compact, molecules can be located only at the intersections between the straight and zig-zag channels and the saturation loading is restricted to 4 molecules per unit cell; see Fig. 1a. The mono-branched 3MP also prefers to locate at the intersections and only at pressures exceeding 10 kPa can these molecules be pushed into the channel interiors. The 3MP isotherm shows strong inflection at four molecules per unit cell. The saturation capacity of 3MP is 6.3 molecules per unit cell, intermediate in value between that of *n*C6 and 22DMB. We also note from Fig. 1a that the dual-site Langmuir (DSL) isotherm (parameters specified in Table 1):

$$\Theta_i^0(p) \equiv \Theta_{i,A} + \Theta_{i,B} = \frac{\Theta_{i,\mathrm{sat},A} b_{i,A} p}{1 + b_{i,A} p} + \frac{\Theta_{i,\mathrm{sat},B} b_{i,B} p}{1 + b_{i,B} p} \tag{5}$$

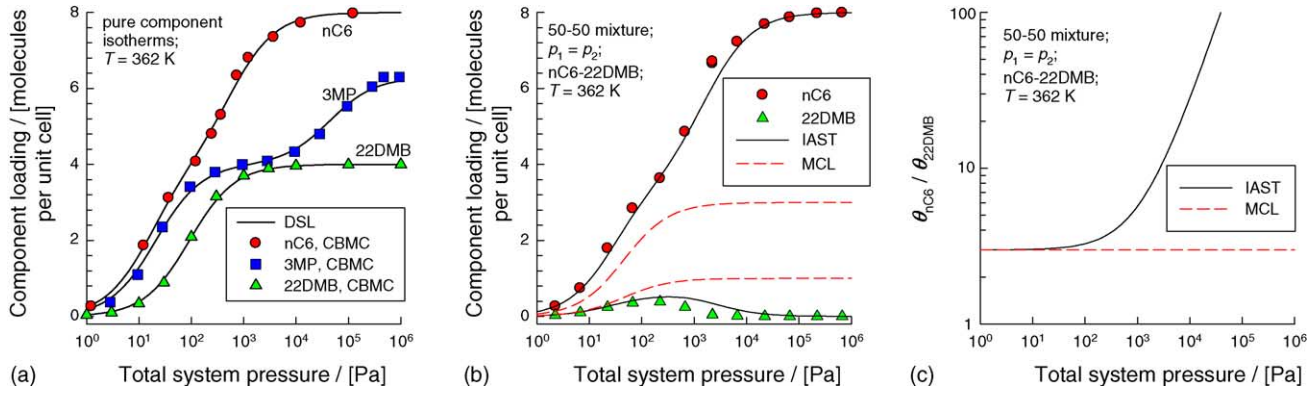

Fig. 1. (a) Pure component sorption isotherms for *n*C6, 3MP and 22DMB in MFI at 362 K. The symbols represent CBMC simulation data [8–10]. The continuous lines are the dual site Langmuir fits using the parameters as specified in Table 1 (b) CBMC simulations (denoted by symbols), of loadings in MFI zeolite at 362 K for 50:50 *n*C6—22DMB mixture. The continuous solid lines in (b) are calculations using IAST, with the DSL parameter inputs as specified in Table 1. The dashed lines in (b) are calculations with the MCL model (3) in which the saturation loadings are taken to be four molecules per unit cell for *both* components and the Langmuir constants b_i are 0.032445 and 0.001085 Pa^{-1} for *n*C6 and 22DMB, respectively. (c) Comparison of the ratio of component occupancies $\theta_{nC6}/\theta_{22DMB}$ predicted by the IAST and MCL approaches.

provides a good description of the pure component isotherms for all three hexane isomers.

The second important limitation of the MCL approach is that Eq. (3) is valid only when the saturation capacities $\Theta_{i,sat}$ are equal for all species; this point has been emphasised by Sircar [13–15]. When the saturation capacities of the constituent species are significantly different, subtle *entropy* effects come into play in determining mixture loadings in zeolites [6–8]. This will be exemplified by considering sorption of a 50:50 binary mixture of *n*C6 and 22DMB in MFI zeolite. The CBMC simulations for this binary mixture are denoted by the symbols in Fig. 1b. It is interesting to note the maximum in the loading of 22DMB when the total mixture loading is four molecules per unit cell, when the intersections are all occupied; this occurs at a total pressure of about 200 Pa. When the pressure is raised above 200 Pa the loading of 22DMB reduces virtually to zero. The *n*C6 has a higher packing efficiency within the MFI matrix than the 22DMB molecules. It is more efficient to obtain higher loading by ''replacing'' the 22DMB with *n*C6; this *configurational entropy* effect is the reason behind the curious maxima in the 22DMB loading in then binary mixture. The configurational entropy effect is captured correctly by the Ideal Adsorbed Solution Theory (IAST), developed by Myers and Prausnitz [16], as is evidenced by the continuous solid lines in Fig. 1b. The good agreement between IAST and CBMC mixture simulations is typical of various mixtures in a variety of zeolite topologies [7,8,10,17].

The application of the MCL model for calculating the component loadings for the 50:50 mixture of *n*C6 and 22DMB is not straightforward. Firstly, the MCL is strictly applicable in a thermodynamically consistent manner when the saturation capacities of the individual components are identical [13–15]; clearly for *n*C6–22DMB mixture this is not true even as an approximation. Secondly, Eq. (3) applies only when the individual species follow the single site Langmuir model. A logical way to apply to MCL model is to calculate the b_i in Eq. (3) from the corresponding DSL parameters using:

$$b_i = \frac{\Theta_{i,sat,A} b_{i,A} + \Theta_{i,sat,B} b_{i,B}}{\Theta_{i,sat,A} + \Theta_{i,sat,B}} \quad (6)$$

From the parameters specified in Table 1, we obtain $b_1 = 0.032445$ Pa^{-1} for *n*C6. Calculations on the component loadings using the MCL Eq. (3), and taking $\Theta_{i,sat} = 4$ for *both* species, are shown with the dashed lines in Fig. 1b. The MCL model is unable to account for the entropy effects prevalent at high mixture loadings and the sorption selectivity is *independent* of total system pressure and mixture loading. The ratio of the component occupancies, $\theta_{nC6}/\theta_{22DMB}$ is

Table 1
Dual-site Langmuir parameters for hexane isomers in MFI at 362 K

Component	Temperature (K)	Dual Langmuir parameters			
		Site A		Site B	
		$b_{i,A}$ (Pa^{-1})	$\Theta_{i,sat,A}$ (molecules per unit cell)	$b_{i,B}$ (Pa^{-1})	$\Theta_{i,sat,B}$
*n*C6	362	6.32×10^{-2}	4.0	1.7×10^{-3}	4.0
3MP	362	4.75×10^{-2}	4.0	2.27×10^{-5}	2.3
2DMB	362	1.085×10^{-2}	4.0	–	–

The fits correspond to BMC simulations [9,10,29].

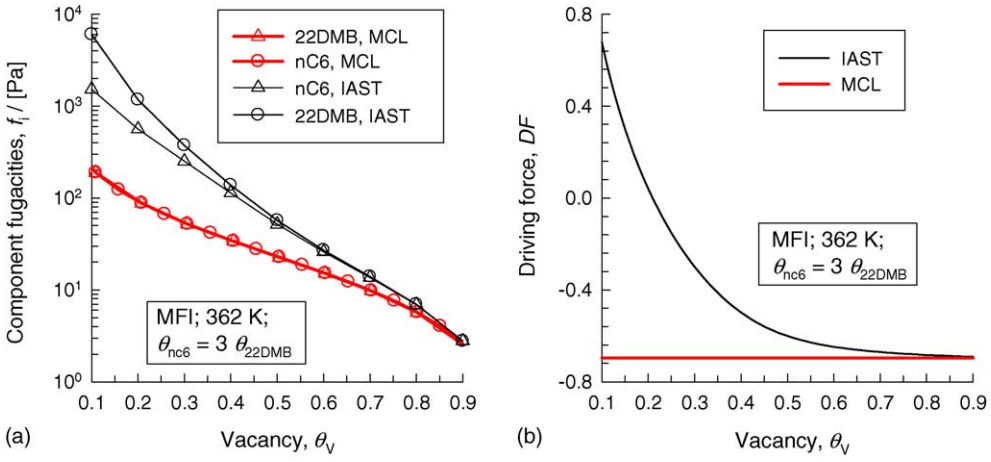

Fig. 2. Comparison of the IAST and MCL predictions of the (a) fugacities f_i of *n*C6 and 22DMB and (b) driving forces DF as a function of the vacancy $\theta_V = 1 - \theta_{nC6} - \theta_{22DMB}$.

predicted to be constant by the MCL approach; see Fig. 1c. The IAST approach predicts a significant increase in $\theta_{nC6}/\theta_{22DMB}$ with increasing total pressure, a consequence of entropy effects.

In Fig. 2a we compare the predictions of the IAST and MCL models of the component fugacities f_i for the case where the ratio of the component occupancies $\theta_{nC6}/\theta_{22DMB}$ is kept constant at a value of 3. As expected the component fugacities coincide for high values of the vacancy $\theta_V = 1 - \theta_{nC6} - \theta_{22DMB}$. The MCL and IAST predictions of p_i diverge significantly for low vacancies θ_V. Note also that the MCL predicts equal fugacities of the two components, whereas the IAST predicts a higher fugacity of 22DMB than that of *n*C6; this is a manifestation of the entropy effect.

The major objective of the present communication is to highlight the importance of entropy effects on the effectiveness factor of zeolite catalysed reactions. We stress the limitations of the LH–MCL approach (i.e. use of Eq. (3)) and put forward a case for a more rigorous LH–IAST approach to the modeling of diffusion limited kinetics; essentially this amounts to using Eq. (2) and evaluation of the occupancies and fugacities within the catalyst employing the IAST. For illustration purpose we consider the reversible isomerization reaction *n*C6 ⇄ 22DMB occurring within an MFI catalyst at a temperature of 362 K. The current work is an extension of our earlier analysis of effectiveness factor for zeolite catalysed reactions in which the components are assumed to follow the MCL adsorption behaviour [18].

2. Diffusion and reaction within a zeolite catalyst

The differential equation describing diffusion and reaction of species i in a spherical crystal is [4,18]:

$$\frac{1}{\delta\xi^2}\frac{\partial}{\partial\xi}(\xi^2 N_i) = \rho q_{i,\mathrm{sat}} \nu_i r \tag{7}$$

where the fluxes N_i are best described by the Maxwell–Stefan (M–S) formulation [19]:

$$\begin{aligned} -\frac{\rho q_{i,\mathrm{sat}}}{\delta}\frac{\theta_1}{RT}\frac{\partial\mu_1}{\partial\xi} &= \frac{\theta_2 N_1 - \theta_1 N_2}{Đ_{12}} + \frac{N_1}{Đ_1} \\ -\frac{\rho q_{i,\mathrm{sat}}}{\delta}\frac{\theta_2}{RT}\frac{\partial\mu_2}{\partial\xi} &= \frac{\theta_1 N_2 - \theta_2 N_1}{Đ_{21}} + \frac{N_2}{Đ_2} \end{aligned} \tag{8}$$

Eq. (8) define two types of Maxwell–Stefan diffusivities: $Đ_i$ and $Đ_{12}$. The $Đ_i$ are the diffusivities that reflect interactions between species i and the zeolite matrix; they are also referred to as jump or "corrected" diffusivities in the zeolite literature [20,21]. The M–S diffusivity displays a wide variety of dependencies on the occupancy, depending on the particular guest–host combination [22,23]. In this paper we consider two special scenarios [24], the *weak confinement* scenario:

$$Đ_i = Đ_i(0) \tag{9}$$

and the strong confinement scenario:

$$Đ_i = Đ_i(0)\theta_V \tag{10}$$

Site-to-site jump leaves behind a vacancy. Subsequent jumps are more likely to fill this vacancy, thus producing "vacancy correlation" effects [25,26]. When the jump of species i creates a vacancy and this vacancy is filled by species j, the vacancy correlation effect is captured by the term containing the "exchange" coefficients $Đ_{12}$ and $Đ_{21}$ in Eq. (8). The net effect of this exchange is a slowing down of a faster moving species due to interactions with a species of lower mobility. Also, a species of lower mobility is accelerated by interactions with another species of higher mobility. For estimation of the $Đ_{ij}$, Skoulidas et al. [24] suggested the logarithmic interpolation formula:

$$\begin{aligned} \Theta_{j,\mathrm{sat}} Đ_{ij} &= [\Theta_{j,\mathrm{sat}} Đ_{ii}]^{\Theta_i/(\Theta_i+\Theta_j)} [\Theta_{i,\mathrm{sat}} Đ_{jj}]^{\Theta_j/(\Theta_i+\Theta_j)} \\ &= \Theta_{i,\mathrm{sat}} Đ_{ji} \end{aligned} \tag{11}$$

where $Đ_{ii}$ are self-exchange coefficients. The interpolation strategy (11) has been verified by comparison with Monte Carlo and Molecular Dynamics simulations [24,25,27]. For facile particle–particle exchange, i.e. $Đ_{ij} \to \infty$, vacancy correlation effects tend to get washed out.

The set of Eqs. (7) and (8) need to be solved numerically to obtain the effectiveness factor for the reaction. We have developed a general purpose code for this purpose; the numerical details have been given elsewhere [28]. We highlight the significant differences between the LH–IAST and LH–MCL approaches in determining the effectiveness factor, η, as a function of the Thiele modulus defined for a spherical catalyst as [4,18]:

$$\phi = \frac{\delta}{3}\sqrt{\frac{k_f}{b_1 Đ_1} + \frac{k_b}{b_2 Đ_2}} \tag{12}$$

For the isomerization reaction *n*C6 ⇄ 22DMB the reaction equilibrium is dictated by the ratio k_f/k_b, that in turn is determined solely by the temperature. All the calculations in presented in this paper are carried out taking $k_f/k_b = 2$, which yields an equilibrium conversion of *n*C6 of 67%. The choice of MCL or IAST does not influence the calculation of the reaction equilibrium but has a significant influence of the loading distribution within the catalyst for diffusion limited reaction. In Fig. 3 we compare the effectiveness factor calculation using the IAST and MCL models, assuming facile exchange i.e. $Đ_{ij} \to \infty$, for varying values of the vacancy at the external surface of the catalyst $\theta_V = 1 - \theta_{s,nC6} - \theta_{s,22DMB}$ while keeping the ratio of the fractional occupancies of the two components at the surface constant, $\theta_{s,nC6} = 3\theta_{s,22DMB}$. In the calculations presented in Fig. 3 the ratio of the zero-loading M–S diffusivities $Đ_1(0)/Đ_2(0) = 10$.

Consider first the weak confinement scenario for both components. From Fig. 3a we note that the LH–MCL approach predicts almost no dependence on the vacancy θ_V. This is in sharp contrast to the LH–IAST approach for which η is strongly reduced when the vacancy is reduced. For example, at $\phi = 1$, $\eta = 0.63$ when $\theta_V = 0.9$ and $\eta = 0.19$ when $\theta_V = 0.1$; this corresponds to a reduction by a factor 3.5. With the LH–MCL for $\phi = 1$, $\eta = 0.68$ when $\theta_V = 0.9$ and $\eta = 0.63$ when $\theta_V = 0.1$. One reason for the significantly lower effectiveness factor for LH–IAST is to be found in Fig. 1c, which shows that the LH–IAST predicts a significantly higher vacancy and, consequently, reaction rates, when the same fugacities of *n*C6 and 22DMB are prevalent in the bulk gas phase.

Fig. 3b compares the effectiveness factor for the LH–IAST and LH–MCL approaches for the strong confinement scenario in which the component M–S diffusivities $Đ_i$ are assumed to follow the dependence described by Eq. (10). In this scenario both IAST and MCL approaches predict a strong reduction in η with decreasing vacancy θ_V; this is primarily due to the reduction in the diffusivity as the vacancy is reduced. For the IAST the effectiveness factor is further lowered below the value predicted by MCL due to the higher reaction rates.

A further reason for the lower effectiveness predicted by IAST may be that the IAST and MCL may anticipate different *directions* in which the reaction proceeds. To demonstrate this let us define the *driving force* for the chemical reaction as:

$$\mathrm{DF} = \ln\left(\frac{k_b}{k_f}\frac{f_2}{f_1}\right) \tag{13}$$

The component fugacities are those prevailing *within* the catalyst particle. For negative DF values, 22DMB is formed

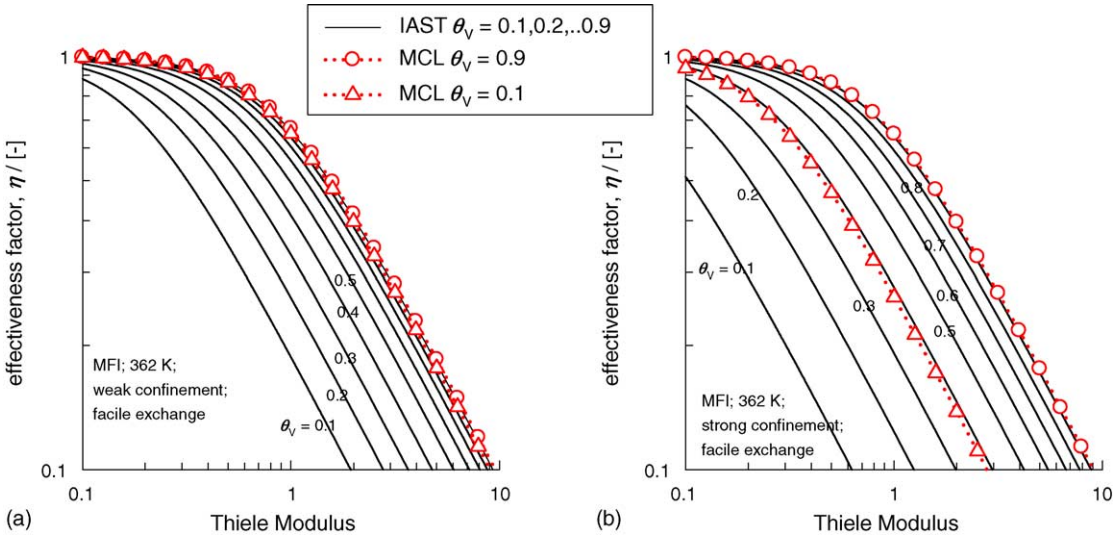

Fig. 3. Effectiveness factor for (a) weak and (b) strong confinement as a function of the Thiele modulus defined by Eq. (12). The fractional loadings at the surface of the zeolite crystal is fixed with $\theta_{s,nC6} = 3\theta_{s,22DMB}$. Also the ratio of the reaction rate constants is fixed at $k_f/k_b = 2$.

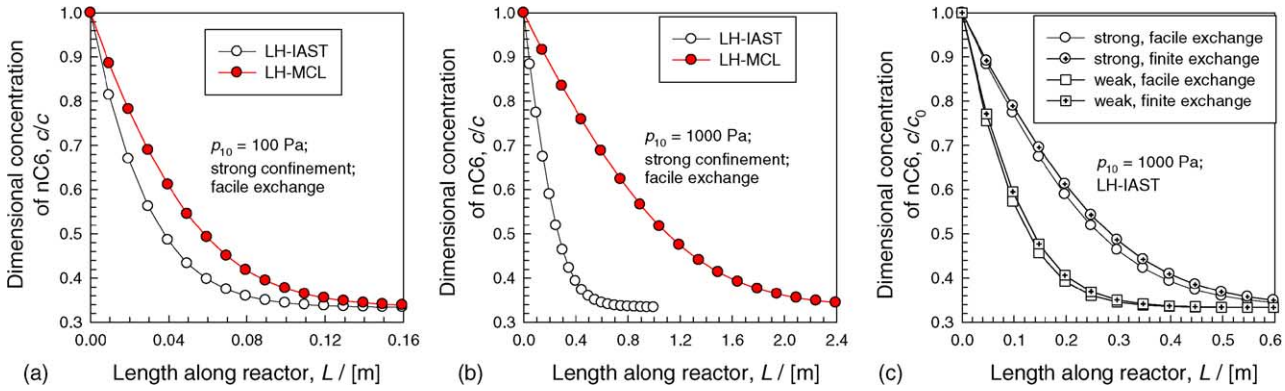

Fig. 4. (a) Comparison of fixed bed isomerization simulations using LH–IAST and LH–MCL models with inlet partial pressure of *n*C6, $p_{10} = 100$ Pa. (b) Comparison of LH–IAST and LH–MCL models with inlet partial pressure $p_{10} = 1000$ Pa. (c) Comparison of various diffusion scenarios for LH–IAST model calculations with inlet partial pressure $p_{10} = 1000$ Pa. The reactor parameters in these simulations are: $k_f = 0.0022852$ Pa^{-1} s^{-1}, $k_b = 0.0011426$ Pa^{-1} s^{-1}, gas velocity at reactor inlet $u_0 = 0.071$ m s^{-1} (this velocity is maintained constant along the length of the reactor), ratio of zero-loading M–S diffusivities $Đ_1(0)/Đ_2(0) = 10$, $Đ_1(0)/\delta^2 = 10^{-4}$ s^{-1}, voidage in reactor $\varepsilon = 0.4$, zeolite density $\rho = 1800$ kg m^{-3}.

whereas positive values indicate 22DMB decomposition, i.e. *n*C6 formation. Chemical equilibrium is reached when the chemical driving force vanishes, i.e. DF = 0. The calculations of DF following the IAST and MCL approaches are shown in Fig. 2b for the case where the ratio of the component occupancies $\theta_{nC6}/\theta_{22DMB}$ is kept constant at a value of 3 and $k_f/k_b = 2$. Let us consider the case where the component occupancies are $\theta_{nC6} = 0.15$ and $\theta_{22DMB} = 0.05$, with a vacancy $\theta_V = 0.8$. The IAST calculations show $f_1 = 6.9$ Pa, $f_2 = 6.97$ Pa and a value of the driving force DF = −0.683 suggesting that the reaction proceeds to the right producing 22DMB, the desired product. For the chosen occupancies the calculations of the MCL yields $f_1 = 5.779$ Pa, $f_2 = 5.76$ Pa and DF = −0.696, a value that is quite close to that anticipated by the IAST. For low occupancies, both IAST and MCL predict nearly the same driving forces and the effectiveness factor of the catalyst are close to each other, as is evidenced by the results presented in Fig. 3.

The situation changes dramatically for high occupancies and for vacancies $\theta_V < 0.2$, the IAST and MCL approaches predict different directions in which the reaction will proceed. Let us consider the case where $\theta_{nC6} = 0.675$ and $\theta_{22DMB} = 0.225$, with a vacancy $\theta_V = 0.1$. The IAST predicts $f_1 = 1525$ Pa, $f_2 = 6003$ Pa and a value of the driving force DF = 0.677 suggesting that the reaction proceeds in the reverse direction with 22DMB decomposition. The corresponding calculations of the MCL yields $f_1 = 208$ Pa, $f_2 = 207$ Pa and DF = −0.696. Thus, in sharp contrast to the IAST the MCL predicts that the reaction proceeds to the right *producing* 22DMB. Thus, for high occupancies the IAST and MCL predict different signs for the driving force. The product decomposition predicted by IAST at high occupancies is the reason for the significantly lower effectiveness factor by this, more rigorous, approach.

In Fig. 4 we illustrate the differences in the LH–IAST and LH–MCL predictions of concentrations profiles in an isomerization fixed bed reactor with pure *n*C6 feed (the reactor parameters are specified in the legend). Firstly, let us consider the inlet feed to be $p_{10} = 100$ Pa. The calculations of the concentration of *n*C6 along the reactor, normalized with respect to the inlet *n*C6 feed concentration, are shown in Fig. 4a for the strong-confinement and facile-exchange scenarios. The numerical details of the reactor calculations are available elsewhere [28]. The differences in the concentration profiles predicted by the IAST and MCL models are not very large because for the chosen inlet feed pressure the occupancies inside the catalyst are low and both approaches predict similar results. The situation changes dramatically at high component loadings; see calculations presented in Fig. 4b for an inlet feed pressure $p_{10} = 1000$ Pa. The LH–IAST approach predicts that the equilibrium conversion is achieved with a reactor length of about 0.6 m. In contrast the LH–MCL approach anticipates that the equilibrium conversion is reached only after a reactor length of about 2.4 m. Even though the LH–IAST predicts a significantly lower effectiveness factor (cf. Fig. 3), the actual reaction rates are predicted to be significantly higher than those anticipated by the LH–MCL model.

The influence of the various diffusion scenarios is illustrated in Fig. 4c for the LH–IAST approach for an inlet feed pressure $p_{10} = 1000$ Pa. The differences between the facile and finite exchange scenarios are found to be insignificant when compared to the differences between the strong and weak confinement scenarios. Put another way, for accurate prediction of the conversion in a fixed bed reactor the occupancy dependence of the M–S diffusivities is of vital importance.

3. Conclusions

For accurate description of adsorption in zeolites of binary mixtures of components of significantly different saturation capacities, we need to adopt the Ideal Adsorbed Solution Theory for estimation of the component loadings

and occupancies, especially for high occupancies (low vacancy). The commonly used multi-component Langmuir approach is not capable of describing the entropy effects that manifest at high loadings. Entropy effects have a significant effect on diffusion controlled chemical reactions taking place within zeolite catalysts. Using a specific example of the isomerization of hexane *n*C6 ⇄ 22DMB in MFI catalyst we have demonstrated the significant differences in the effectiveness factor anticipated by the LH–MCL and LH–IAST approaches. The differences in these two approaches increases at high component occupancies. In a fixed bed reactor The LH–MCL approach predicts a significantly higher reactor length to achieve equilibrium conversion than that anticipated by the LH–IAST approach. Our study also emphasizes the need for an accurate description of the loading dependence of the M–S diffusivity $Đ_i$.

Acknowledgement

RB and RK acknowledge a grant *Programmasubsidie* from the Netherlands Foundation for Fundamental Research (CW-NWO) for development of novel concepts in reactive separations.

References

[1] A. Corma, J. Catal. 216 (2003) 298–312.
[2] T.F. Degnan, J. Catal. 216 (2003) 32–46.
[3] C. Marcilly, J. Catal. 216 (2003) 47–62.
[4] R. Aris, The mathematical theory of diffusion and reaction in permeable catalysts, Clarendon Press, Oxford, 1975.
[5] D. Dubbeldam, S. Calero, T.J.H. Vlugt, R. Krishna, T.L.M. Maesen, E. Beerdsen, B. Smit, Phys. Rev. Lett. 93 (8) (2004) (Art. No. 088302).
[6] F. Kapteijn, J.A. Moulijn, R. Krishna, Chem. Eng. Sci. 55 (2000) 2923–2930.
[7] R. Krishna, S. Calero, B. Smit, Chem. Eng. J. 88 (2002) 81–94.
[8] R. Krishna, B. Smit, S. Calero, Chem. Soc. Rev. 31 (2002) 185–194.
[9] S. Calero, B. Smit, R. Krishna, J. Catal. 202 (2001) 395–401.
[10] M. Schenk, S.L. Vidal, T.J.H. Vlugt, B. Smit, R. Krishna, Langmuir 17 (2001) 1558–1570.
[11] D. Dubbeldam, S. Calero, T.J.H. Vlugt, R. Krsihna, T.L.M. Maesen, B. Smit, J. Phys. Chem. B 108 (2004) 12301–12313.
[12] T.J.H. Vlugt, R. Krishna, B. Smit, J. Phys. Chem. B 103 (1999) 1102–1118.
[13] S. Sircar, AIChE J. 41 (1995) 1135–1145.
[14] S. Sircar, M.B. Rao, AIChE J. 45 (1999) 2657–2661.
[15] M.B. Rao, S. Sircar, Langmuir 15 (1999) 7258–7267.
[16] A.L. Myers, J.M. Prausnitz, AIChE J. 11 (1965) 121–130.
[17] R. Krishna, R. Baur, Chem. Eng. Sci. 60 (2005) 1117–1126.
[18] R. Baur, R. Krishna, Chem. Eng. J. 99 (2004) 105–116.
[19] R. Krishna, J.A. Wesselingh, Chem. Eng. Sci. 52 (1997) 861–911.
[20] D.M. Ruthven, Principles of Adsorption and Adsorption Processes, John Wiley, New York, 1984.
[21] J. Kärger, D.M. Ruthven, Diffusion in Zeolites and Other Microporous Solids, John Wiley, New York, 1992.
[22] A.I. Skoulidas, D.S. Sholl, J. Phys. Chem. A 107 (2003) 10132–10141.
[23] R. Krishna, D. Paschek, R. Baur, Microporous Mesoporous Mater. 76 (2004) 233–246.
[24] A.I. Skoulidas, D.S. Sholl, R. Krishna, Langmuir 19 (2003) 7977–7988.
[25] R. Krishna, D. Paschek, Phys. Chem. Chem. Phys. 4 (2002) 1891–1898.
[26] J. Kärger, S. Vasenkov, S.M. Auerbach, Diffusion in zeolites, in: S.M. Auerbach, K.A. Carrado, P.K. Dutta (Eds.), Handbook of Zeolite Science and Technology, Marcel Dekker, New York, 2003 (Chapter 10).
[27] R. Krishna, Chem. Phys. Lett. 355 (2002) 483–489.
[28] R. Krishna, R. Baur, Diffusion Adsorption and Reaction in Zeolites: Modelling and Numerical Issues, University of Amsterdam, Amsterdam, 10 November 2003 http://ct-cr4.chem.uva.nl/zeolite.
[29] R. Krishna, R. Baur, Sep. Purif. Technol. 33 (2003) 213–254.